

Analysis of C-Band Radar Temporal Coherence Over an Irrigated Olive Orchard in a Semi-Arid Region

Adnane Chakir¹, Pierre-Louis Frison², Ludovic Villard³, Nadia Ouaadi⁴, Pascal Fanise⁵, Khabba Saïd⁶, Valérie Le Dantec⁷, Rafi Zoubair⁸, Jamal Ezzahar⁹, Bénédicte Fruneau¹⁰, Jean-Paul Rudant¹¹, and Jarlan Lionel¹²

Abstract—This article aimed to monitor vegetation using C-band radar data at a subdaily time step. To this end, radar measurements using tower-mounted antennas with a 15-min time step, along with physiology-related information (sapflow and micrometric dendrometry), were acquired quasi-continuously from March 2020 to December 2021 in an olive orchard located near Marrakech, Morocco. The article focused on temporal coherence, whose clear diurnal cycle (highest at night and lowest at the end of the afternoon) had been highlighted over tropical and boreal forests in previous studies. The results showed that coherence was highly sensitive to: wind-induced movement of scatterers, since coherence was lowest when wind speed was highest in late afternoon, and vegetation activity, especially its water dynamics, since the morning coherence drop coincided with the onset of sapflow and the daily evapotranspiration cycle, as well as the good agreement between the temporal drop rate of coherence and the daily residual variation in trunk circumference (i.e., deviation from long-term trend). Finally, coherence remained high for temporal baselines of several days, showing that sentinel-1 data (when both satellites are operational)

may be well suited for such studies, especially with acquisitions made during morning passes, when wind speed is low. These results open perspectives for monitoring tree crop physiology using high-revisit-time radar observations.

Index Terms—C-band, olive orchard, radar, temporal coherence, water status.

I. INTRODUCTION

SINCE semiarid regions have evaporative demand that far exceeds rainfall, crops there rely mainly on irrigation. Due to recurrent droughts [1], [2] and demographic pressure, which leads to increasing demand for agricultural production [3], these regions are facing a drastic decrease in their water resources [4]. It is therefore essential to manage water sustainably and thus use irrigation rationally [5], [6]. To achieve this objective, monitoring the water status of crops regularly is of prime importance.

Visible and near-infrared data are key observations for monitoring crop health and photosynthetic activity; however, they detect water stress several days after it occurs, when crops may have already been irreversibly damaged. In contrast, thermal infrared data have been used extensively to detect water stress earlier, since surface temperature is an indirect proxy of the water status of vegetation when water is limiting [7], [8], [9]. Unfortunately, data that combine high resolution and high revisit time in the thermal infrared domain will not be available until the launch of the future missions TRISHNA and LSTM. In contrast, radar data that are sensitive to plant and soil water content can directly assess the water status of vegetation [10], [11]. In particular, their sensitivity to diurnal variations in plant water has already been highlighted for tropical rainforests by analyzing contrasting radar responses [12], [13]. The launch of the sentinel-1 missions represented an unprecedented improvement in land-surface monitoring by radar remote sensing, since they provided, for the first time, a short revisit time (6 or 12 days, depending on the region) with a spatial resolution of about 10 m. They are particularly well suited for monitoring seasonal land-surface variations at local and regional scales [8], [14], [15]. However, using these data to assess the water status of vegetation and, to a larger extent, to interpret temporal signatures in relation to seasonal variations, remains questionable. For this reason, a tower-based radar experiment was conducted over an olive orchard in an agricultural field in Morocco [16] in which tower-mounted antennas have acquired C-band radar measurements with a 15-min time step since Mar 2020. These radar measurements, along with other measurements (e.g.,

Manuscript received 27 September 2023; revised 24 November 2023 and 20 December 2023; accepted 2 January 2024. Date of publication 11 January 2024; date of current version 29 January 2024. This work was supported in part of the CNES-TOSCA MOCTAR project, in part by LMI TREMA (UCA-IRD), in part by ERANET-MED CHAAMS, and in part by H2020 RISE ACCWA Projects, as well as the PHC Toubkal Program. (Corresponding author: Adnane Chakir.)

Adnane Chakir is with the LMFE, Faculty of Sciences Sémmlalia, Cadi Ayyad University, Marrakech 40000, Morocco, and also with the LaSTIG, Université Gustave Eiffel, ENSG, IGN, 77420 Champs-sur-Marne, France (e-mail: adnane.chakir@ird.fr).

Pierre-Louis Frison is with the LaSTIG, Université Gustave Eiffel, ENSG, IGN, 77420 Champs-sur-Marne, France, and also with the Centre d'Études Spatiales de la Biosphère, 31401 Toulouse, France (e-mail: pierre-louis.frison@u-pem.fr).

Bénédicte Fruneau and Jean-Paul Rudant are with the LaSTIG, Université Gustave Eiffel, ENSG, IGN, 77420 Champs-sur-Marne, France (e-mail: benedicte.fruneau@u-pem.fr; jean-paul.rudant@u-pem.fr).

Ludovic Villard, Pascal Fanise, and Jarlan Lionel are with the Centre d'Études Spatiales de la Biosphère, 31401 Toulouse, France (e-mail: ludovic.villard@cesbio.cnes.fr; pascal.fanise@ird.fr; jarlan.lionel@gmail.com).

Nadia Ouaadi is with the Centre d'Études Spatiales de la Biosphère, 31401 Toulouse, France, and also with the CNRM, Météo France Toulouse, 31057 Toulouse, France (e-mail: nadia.ouaadi@gmail.com).

Khabba Saïd is with the LMFE, Faculty of Sciences Sémmlalia, Cadi Ayyad University, Marrakech 40000, Morocco, and also with the CRSA, Mohammed VI Polytechnic University, Ben Guerir 43150, Morocco (e-mail: khabba@uca.ac.ma).

Valérie Le Dantec is with the Biogeosciences Département, Toulouse III Paul Sabatier University, 31062 Toulouse, France (e-mail: valerie.le-dantec@univ-tlse3.fr).

Rafi Zoubair is with the Institute of Research for Development, Marrakech 40000, Morocco (e-mail: zoubairafi@gmail.com).

Jamal Ezzahar is with the MISCOM, National School of Applied Sciences, Cadi Ayyad University, Marrakech 40000, Morocco, and also with the CRSA, Mohammed VI Polytechnic University, Ben Guerir 43150, Morocco (e-mail: j.ezzahar@uca.ma).

Digital Object Identifier 10.1109/JSTARS.2024.3352699

temperature and humidity) that characterize surface conditions, provide a unique opportunity to better understand the influence of surface parameters on radar response. This article focused on temporal coherence: the complex correlation between two radar acquisitions with similar geometry. It indicates the stability of the elementary scatterers (e.g., leaves, stems) within a set of pixels in terms of dielectric permittivity and geometrical features. Thus, coherence is sensitive to variations in the water content and geometry (i.e., position and orientation) of the scatterers on the scale of a few fractions of the wavelength (< 1 cm in the *C*-band). Previous studies have analyzed the coherences obtained with similar experiments over tropical forests (TF) and boreal forests (BF) [17], [18], [19], [20], [21]. They show that although temporal coherence decreases with the radar wavelength (higher in the *P*-band than in the *C*-band), it has a distinct diurnal cycle related to the wind and water flow in plants [related to evapotranspiration (ETR)].

The present article aimed to verify whether these observations could be confirmed in the *C*-band over an olive orchard, and if so, whether temporal coherence could provide information about the water status of the tree canopy. Since previous studies have shown that dew and rainfall intercepted by vegetation directly decrease coherence, and both are particularly rare in the study region, the study focused on the effects of plant water content on coherence.

II. STUDY SITE AND EXPERIMENTAL DATA

A. Study Site

The study site was located in the Chichaoua region, 70 km west of Marrakech, on the Haouz plain (central Morocco). It has a semi-arid Mediterranean climate, with ETR of *ca.* 1600 mm/year and rainfall of < 250 mm/year. Under these conditions, irrigation is crucial for agricultural activity. Recurrent droughts since the early 2000s, combined with the continued increase in water demand, especially for irrigation, have led to groundwater depletion of 0.5–3.0 m/year [22]. Of the irrigated land on this plain, 51% is used to grow cereals, and 38% is used to grow trees, mainly olives (78%) [23]. The rest of the plain (unirrigated), which covers 4000 km² (twice the size of the irrigated area), is used almost exclusively to grow rainfed wheat [23]. A 2.4 ha olive orchard was instrumented with radar and many other sensors (see Fig. 1). The olive orchard contained 40 rows with 11 olive trees each (i.e., one tree per 7.5 x 7.5 m²), *ca.* 20 years old and 3 m tall, planted on a clay-loam soil with a drip irrigation system.

B. Physiological and Meteorological Data Collection

The study site was equipped with instruments that measure the state of the surface. A weather station measured air humidity and temperature, incoming radiation and wind speed every 30 min. In addition, convective latent and sensible heat fluxes were measured using an eddy covariance system with a high-frequency anemometer (CSAT, Campbell Scientific, Logan, Utah, USA) and a Krypton hygrometer gas analyzer (KH20, Campbell Scientific) [24]. Finally, tree physiological functioning was monitored using a sapflow thermal dissipation probe (TDP-50, Dynamax,

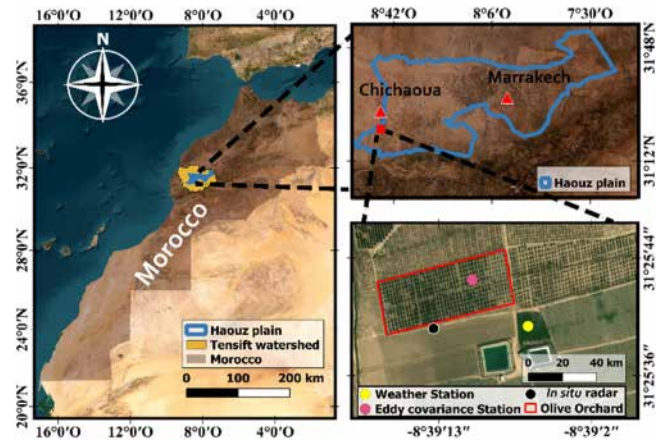


Fig. 1. Location of the studied olive orchard on the Haouz plain, central Morocco.

Houston, Texas, USA) [25] and micro-metric dendrometry of the trunk circumference using a strain gauge. To this end, two sapflow sensors and one dendrometer were installed on each of the four olive trees located around the eddy covariance station. The sensors were placed next to each other to ensure that sapflow and circumference measurements represented the same section of the trunk. The thermal dissipation probe method is based on Granier's heat-balance method for measuring xylem sap flow. The work in [26] and [27] give details about processing and correcting sapflow measurements. Dendrometer data were processed using the "dendRoAnalyst R" package of R software [28] and used to calculate the daily residual variation in tree circumference (i.e., deviation from long-term trend). The work in [29] gives detail about processing dendrometer data.

The timing and amount of irrigation events were also recorded during the study. Unfortunately, time-domain reflectometry probes (type: CS655) placed in two pits at multiple depths (5–80 cm) could not detect changes in soil surface water content due to irrigation since they had not been placed near the pipes of the drip irrigation system. Irrigation practices differed between 2020 and 2021: in 2020, *ca.* 1.5 mm of water was applied each day, which resulted in high soil evaporation and thus water stress for the olive trees. To remedy this problem, in 2021 all trees were irrigated with the same cumulative amount of water (3.0–3.5 mm) every 2–3 d (depending on other crop activities), which decreased water stress greatly.

C. Tower-based Radar System

Radar measurements were performed using a vector network analyzer (VNA) with two ports (type: s5065 [30]), three electromechanical duplexers, nine low-loss coaxial cables 3 m long (type: FSJ1RN-50B) and seven *C*-band horn antennas (type: LB-159-10-C-NF). The VNA was installed on the top of a 20 m tower located at the central edge of the olive orchard (Fig. 2). This experiment continuously acquired radar signals from March 2020, with a time step of 15 min. A total of 20 months (i.e., until Dec 2021) of continuous *C*-band acquisitions were available, with short interruptions due to hardware problems.



Fig. 2. Photographs of the experimental site and the antenna array at the top of the tower. The seven small antennas in the top frame are those operating in the C-band.

TABLE I
HORN ANTENNA PARAMETERS USED FOR THE C-BAND ACQUISITIONS (5.2–5.8 GHz)

| Frequency (GHz) | Gain (dB) | Antenna factor (dB/m) | Cross-polarization isolation (dB) | V- and H-plane beamwidths 3 dB |
|-----------------|-----------|-----------------------|-----------------------------------|--------------------------------|
| 5.0 | 10.51 | 33.68 | -32 | 56.77° and 55.16° |
| 5.5 | 10.95 | 34.07 | -40 | 54.45° and 49.93° |
| 6.0 | 11.63 | 34.14 | -44 | 50.57° and 46.56° |

The VNA was connected via the electromechanical duplexers to seven C-band horn antennas (two transmitting and five receiving) in two polarizations [four in vertical (V) and three in horizontal (H) polarization]. The seven antennas are arranged on three levels (four at the bottom, three in the middle, and one at the top, Fig. 2). The bottom and top levels are 50 and 30 cm, respectively, from the middle one, with horizontal spacing of 30 cm between the antennas. Each pair of antennas formed a receive-transmit pair, which allowed for acquisition in VV, VH, HV, and HH polarizations. Although four antennas (two pairs in V and H polarizations for transmission and reception) are sufficient for acquisitions in all polarizations, three additional receiving antennas have been installed. This is done both to minimize risks associated to failures and malfunctions, and to enhance coherence estimation by combining polarization configurations (see the end of Section II-C). The corresponding maximum gains and beamwidths varied (see Table I). The antennas were directed towards the orchard with an angle of incidence $\theta = 55^\circ$.

The measurements were acquired in the frequency domain. Each complex scattering amplitude (i.e., scattering matrix element [31]) $S(f)$ consisted of $N_f = 1601$ consecutive frequency points (complex measurements) sampled at a rate of $F_s = 1$ kHz, over the frequency interval $B = 5.2$ –5.8 GHz with a frequency step $\delta f = \frac{B}{N_f - 1} = 375$ kHz (corresponding to a range ambiguity $\Delta r = \frac{c}{2\delta f} = 400$ m), for a total duration of $T = N_f / F_s = 1.6$ s. After applying a Hamming filter, the complex range profile $S(t)$ was converted using an inverse Fourier transform over 8192 samples, which resulted in a pixel size and spatial resolution of *ca.* $\delta p = 5$ cm and $\delta r = 27$ cm in slant range (i.e., the natural geometry of radar acquisition), to be compared to the highest possible resolution of $c / 2B = 25$ cm without the windowing filter.

This study focused on olive trees in the range of $r_{\min} = 25$ to $r_{\max} = 40$ m, corresponding to incidence angles of *ca.* $\theta_{\text{Near}} \approx$

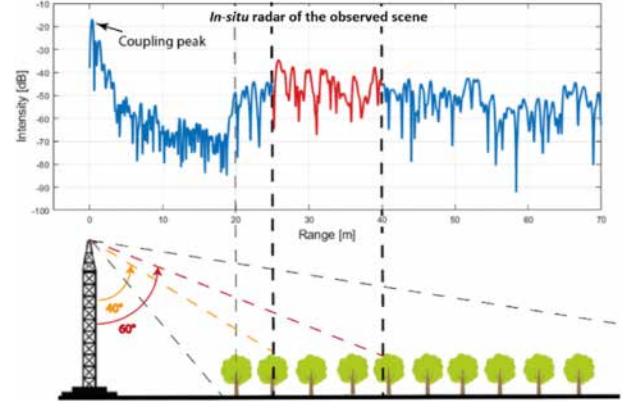


Fig. 3. Magnitude squared of a backscattered radar response in (i.e., $|S(t)|^2$) in function of range, with an illustration of how the tower-based radar wave relates to a two-dimensional slice of the observed scene. The region with dynamics in red shows the range of 25–40 m over which the radar response was analyzed over olive trees. The range scales are not the same as the upper figure is shown in slant geometry, with the origin at the antenna, while the lower one is shown in ground geometry.

40° to $\theta_{\text{Far}} \approx 60^\circ$ (see Fig. 3). This resulted in a pixel size δp_g and spatial resolution δr_g of 5.6–7.6 cm and 31–42 cm in ground geometry, respectively, after the projection of the radar line of sight onto the horizontal ground surface by dividing δp and δr by $\sin(\theta)$ [32]. The azimuthal resolution was determined by $\delta a = \beta_{3\text{dB}} \cdot R$, where $\beta_{3\text{dB}} \approx 55^\circ$ is the beamwidth in the azimuthal direction (see Table I) and R is the distance to a given cell. For distances of 25–40 m, the azimuthal resolution was thus $\delta r_{az} = R \cdot \beta_{3\text{dB}} \approx 24$ –38 m. An illustration of an acquired range profile $|S(t)|^2$ as a function of distance with the acquisition diagram is shown in Fig. 3.

For a given pair of antenna configurations, three successive acquisitions (sequence A, B, and C) were performed. Ultimately, a total cycle of 30 acquisitions (i.e., 3 sequences \times 10 antenna pair configurations) was performed in a little more than 1 min. Before each 15 min. acquisitions cycles, the time variant losses (especially due to temperature) in the RF cables are updated and accounted for by the VNA, considering a specific line made with interconnected transmitting and receiving cables of the same length. For each antenna pair configuration, each backscattered pulse was corrected twice against an arbitrarily chosen reference measurement [32]: phase shift of the coupling between the antennas and the tower and relative calibration of the backscattered power (see Fig. S1). After these corrections, we excluded the two HV pairs and one VH pair due to their unexpected temporal variability, which left seven pairs: three in VV, two in HH and two in VH polarization.

For the polarization pq , temporal coherence for a baseline $\Delta t = t_2 - t_1$ was estimated as follows:

$$\rho_{pq} = \frac{\langle S_{pq}^{k,s,r}(t_1) \cdot S_{pq}^{k,s,r}(t_2)^* \rangle_{k,s,r}}{\sqrt{\langle S_{pq}^{k,s,r}(t_1) \cdot S_{pq}^{k,s,r}(t_1)^* \rangle_{k,s,r}} \cdot \sqrt{\langle S_{pq}^{k,s,r}(t_2) \cdot S_{pq}^{k,s,r}(t_2)^* \rangle_{k,s,r}}} \quad (1)$$

where the brackets notation means the multilook over the antenna pairs (k), the sequences (s), and the range bins (r), that is

$$\begin{aligned} & \langle S_{pq}^{k,s,r}(t_1) \cdot S_{pq}^{k,s,r}(t_2)^* \rangle_{k,s,r} \\ &= \sum_{k=1}^K \sum_s^{A,B,C} \sum_{r=r_{\min}}^{r_{\max}} S_{pq}^{k,s,r}(t_1) \cdot S_{pq}^{k,s,r}(t_2)^* \end{aligned}$$

where $S_{pq}^{k,s,r}(t_1)$ is the complex range profile element measured at time t_1 and its conjugate $S_{pq}^{k,s,r}(t_2)^*$ at time t_2 .

This article analyzed the magnitude $|\rho|$, whose accuracy depends on the equivalent number of looks (ENL). For the 7 pairs of antenna configurations, 3 sequences, and 55 cells with a resolution of 27 cm included in the range interval $\Delta r = r_{\max} - r_{\min} = 15$ m, we expected a maximum ENL of 1155, assuming complete decorrelation between the three sequences. Given the temporal correlation between measurements, we estimated an ENL of 180 (nighttime) to 220 (daytime), with a median of *ca.* 200. Regardless of whether the estimates were based on the traditional square of the ratio of the mean to the standard deviation [33] or on interdependent antenna pair configurations [32], the same results were obtained. Consequently, the bias associated with the estimated coherence was considered negligible (for $|\rho| > 0.2$) or less than 0.1 (for $|\rho| < 0.2$) [34].

D. Sentinel-1 Acquisitions

The tower-based radar acquisitions were compared to sentinel-1 data. To this end, interferometric wide mode images were downloaded in single-look complex format to estimate temporal coherence in VV and VH polarizations with a time step of 6 d (i.e., between two successive acquisitions). These products have a spatial resolution of $3 \text{ m} \times 22 \text{ m}$ and a pixel size of $2.3 \text{ m} \times 14 \text{ m}$ in slant range and azimuth directions, respectively. Of the three orbits that acquired images of the study site, two were selected: no. 118 (ascending), because its incidence angle of observation ($\theta = 45^\circ$) was closest to those of tower-based radar measurements (40° – 60°), with an acquisition time of 18:41, and no. 52 (descending), with a lower incidence angle ($\theta = 35^\circ$) but an acquisition time of 06:36, which corresponded to the highest temporal coherences.

Temporal coherence (over a window size of 15×3 pixels in range and azimuth) was estimated using the SNAP toolbox provided by the European Space Agency [35]. After projecting the coherence image into the geographical system used (UTM 29 N), the 125 pixels of the olive field were averaged to calculate coherence at the field scale.

III. RESULTS

A. 15 Min Temporal Baseline

Daily dynamics of coherence with a 15-min baseline for three two-month periods, which corresponded roughly to three phenological stages [i.e., flowering and fruit set in spring (April–May), pit hardening in summer (July–August) and fruit ripening in autumn (October–November)], has been estimated for the years

2020 and 2021 (see Figs. S3 and 4, respectively). Coherence ($|\rho|$) was estimated for all seven antenna pair combinations since similar behavior was observed when polarization configurations were considered separately. Coefficients of determination (r^2) between coherences in VV, HH and VH polarizations were high (≥ 0.87), regardless of the two-month period considered, and they increased (to 0.99) when only daily median coherences were considered (see Fig. S3 for July–August 2021 illustration). These results show a bare dependence of coherences on polarization. The potential cross-talk effects due to the proximity between the antennas forming the array, seem to be not strong enough to explain such a phenomenon, as shown by the low coherence values between co- and cross-polarization pairs in Fig. S3 (mean, standard deviation and maximum of 0.13, 0.007, and 0.47, respectively). This aspect will be clarified in future studies. In the present study, we prefer to mix them together as looks and we compute the ad-hoc generalized coherence (combination of polarizations as different looks) hereinafter to get more precise estimations (see Section II-C).

Overall, diurnal cycles were similar for all three two-month periods (see Fig. 4). Coherence was high (≈ 1) at night, when the wind speed (W) was low and the vegetation at rest. At dawn (determined by positive net radiation), coherence decreased, reaching its lowest value in late afternoon (when W was highest) and then increasing again to high nighttime values, beginning near sunset (see Fig. 4). The dawn drop coincided with the onset of vegetation activity, as illustrated by the increase in sapflow and real ETR while W was low (until median W exceeded 2 m/s, at *ca.* 10:00–11:00) (see Fig. 4).

During spring and summer, which had higher W , W , and coherence exhibited opposite symmetrical trends, with plateaus and extremes coinciding in time, which reflects the sensitivity of coherence to the movement of vegetation by the wind. Seasonal dynamics revealed the lowest amplitude of the diurnal cycle of coherence during olive orchard dormancy in October–November, in agreement with the lowest amplitudes of diurnal cycles of ETR, sapflow and residual variation in trunk circumference. This period also had the lowest W . Furthermore, at the end of the day, coherences returned to nighttime values, while W remained high at *ca.* 2 m/s. Similar behavior was observed in spring and summer, but with significantly higher amplitude of the diurnal cycle of ETR and sapflow, and a longer active period due to a longer daylength.

The high sensitivity of coherence to W was corroborated by a significant r^2 of 0.60 between them for $W \geq 2$ m/s for all of 2021. This sensitivity to scatterer movement induced low r^2 between $|\rho|$ and ETR and sapflow ($r^2 = 0.10$ and 0.22 , respectively) for the entire daytime period. However, when measurements associated with $W > 2$ m/s were filtered out (on a selection of days with $W < 2$ m/s, $> 50\%$ of daytime only), r^2 reached 0.40 and 0.47, respectively, highlighting the sensitivity of $|\rho|$ to physiological mechanisms of plants. The influence of irrigation events was also investigated by separating the days with irrigation from the days without irrigation, and the coherence of their diurnal cycles did not differ (data not shown).

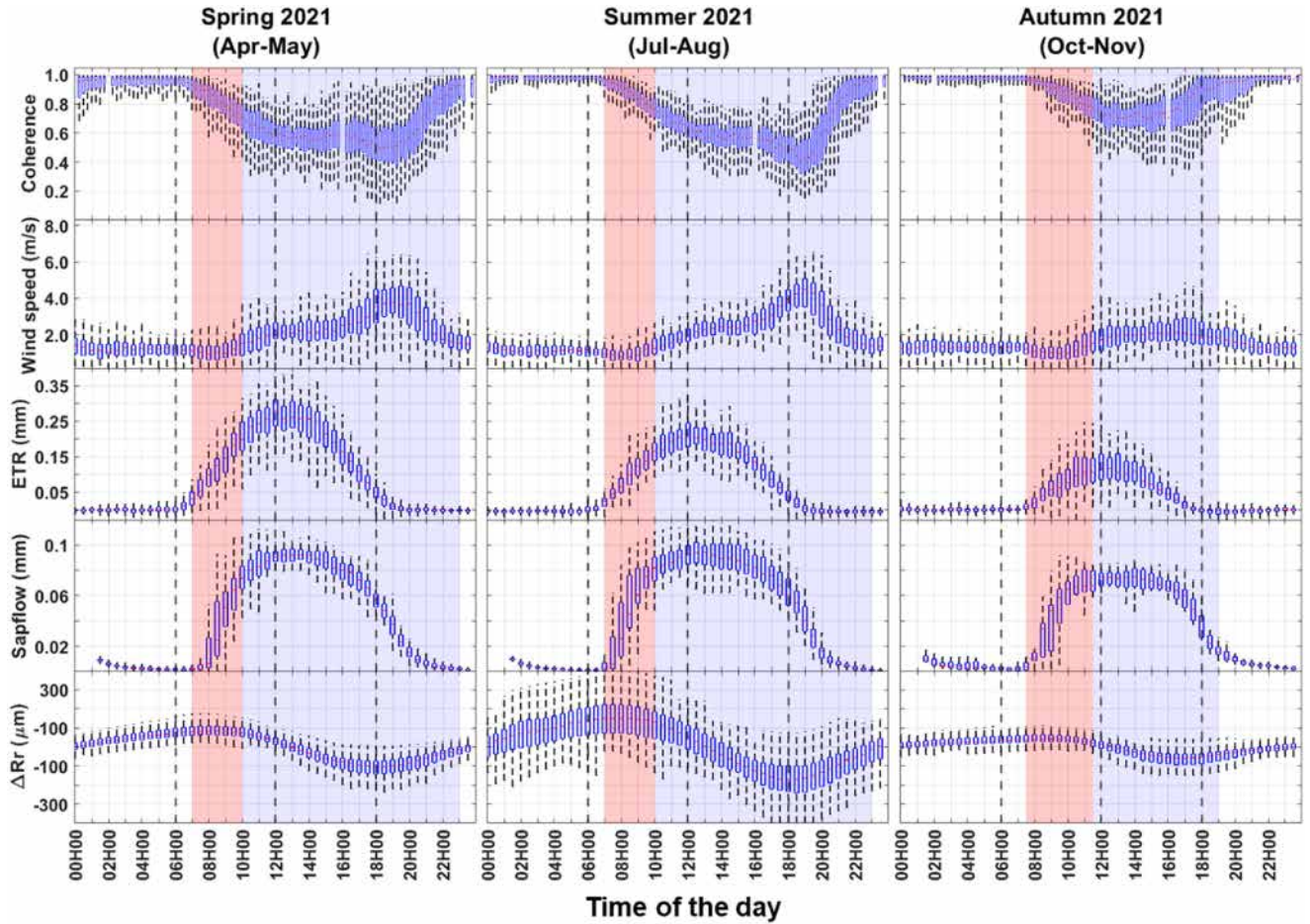


Fig. 4. Daily dynamics as boxplots (error bars are min and max) of (from top to bottom): 15-min coherences, ETR, wind speed (W), sapflow, and residual variation in trunk circumference (ΔRr). From left to right: results for three two-month periods of 2021 reduced to a 24 h scale. Red zones indicate the hours after dawn until median wind speed exceeded 2 m/s. Blue zones indicate the remainder of the daytime period (until median wind speed was lower than 2 m/s).

The diurnal cycle of the residual variation in trunk circumference was shifted compared to those of the other variables. It increased from twilight to *ca.* 2 h after dawn (i.e., trunk rehydration) and then began to decrease slightly after sapflow increased. Likewise, sapflow peaked *ca.* 4 h before the residual variation in trunk circumference reached a minimum in the late afternoon, a common behavior that has been observed in previous studies [36]. The daily residual variation in trunk circumference is assumed to indicate a plant's daily hydrological functioning better than early morning ETR or sapflow, which are governed primarily by available energy in the absence of water stress [37]. The time series of the morning (i.e., the 3 h after dawn) slope of the temporal coherence was examined, since the drop rate in the morning is expected to be related to: the water status of plants and the time series of the daily residual variation in trunk circumference. A Savitsky–Golay filter (polynomial of degree 5 and frame length of 7 d) was also applied to the coherence and circumference data to decrease the amount of noise. The residual variation in trunk circumference showed a clear seasonal signal, with low values during dormancy (winter to early spring) and increasing values from early May to the end of September (see Fig. 5). During this growing period, the residual variation in trunk circumference alternated between

increasing and decreasing for several consecutive days each (see Fig. 5). In contrast, the coherence slope varied more but had the lowest absolute value in winter, as expected. Based on visual inspection, increases in the daily residual variation in trunk circumference tended to correspond well to the temporal rate of coherence drop, except for certain consecutive-day periods (mainly that in July 2020). During the active growing period (May–August 2021), the coherence slope and residual of the trunk circumference had correlations (r) of -0.39 and -0.71 ($n = 109$ points) for raw and filtered values, respectively, and both were significant ($p < 0.01$, Student's t -test). Thus, the morning coherence drop could be attributed to water movement in the xylem, which opens perspectives for monitoring plant water status using C-band radar data.

B. Baselines of Multiple Days

To investigate the potential use of temporal coherence to monitor vegetation using spaceborne data, we analyzed its temporal dynamics for different temporal baselines ($\Delta t = t_2 - t_1$), mimicking the revisit time of sensors in orbit from 0–30 d, with a time step of 15 min. We calculated all the possible combinations of dates matching a given time interval Δt spanning from 15

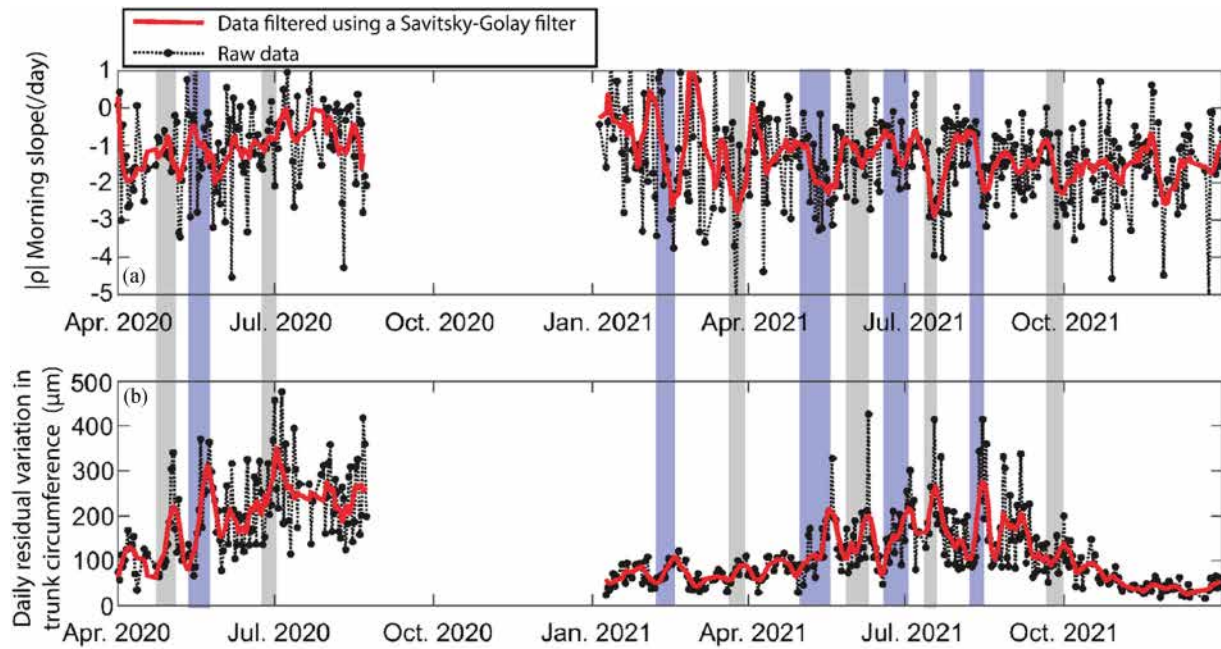


Fig. 5. (a) Morning (i.e., the 3 h after dawn) slope of temporal coherence. (b) daily residual variation in trunk circumference, showing raw data and data filtered using a Savitsky–Golay filter. Alternating gray and blue vertical strips (the change of color is for clarity) highlight several consecutive days of increasing trunk circumference. The time series from September–December 2021 was excluded due to missing data.

min. to 30 days with a time step of 15 min., with t_1 set to 00:00. The resulting median coherence (as well as standard deviation) for the corresponding 2-month periods analyzed previously is shown in Fig. 6. The diurnal cycles observed previously (with peaks at night) were convolved, with a generally exponential decrease that was strongest in spring 2021 ($|\rho| \leq 0.3$ for $\Delta t \geq 6$ d and $|\rho| \approx 0.1$ for $\Delta t \geq 15$ d), likely due to more plant activity and growth in spring than in autumn, which increased the loss of coherence between acquisitions (see Fig. 6). The overall decrease was smoother in summer 2021, with $|\rho_{\max}| \geq 0.3$ for $\Delta t \leq 17$ d and well-defined diurnal cycles, even for long temporal baselines. The decorrelation loss of coherence was smallest and more linear in autumn [see Fig. 6(c)] and winter (data not shown) 2021, which had little or no plant activity. The coherence remained high in autumn 2021 ($|\rho| \geq 0.3$ for $\Delta t \leq 30$ d), for which only 13 coherences were calculated, with t_1 chosen at 00:00 from October 1–13. After October 13, the baseline included November 11, the date of olive harvest, when coherence decreased greatly [see Fig. 7(a)]. This illustrates the sensitivity of coherence to small vegetation scatterers, since olive harvesting involves only cutting the olives off without significantly changing the structure of the tree, especially the leaves, which must not be torn off.

Coherence showed similar trends with baselines of $\Delta t = 15$ min in 2020 (see Figs. 4 and S2), although some differences became apparent with baselines of up to 30 d. Temporal signatures of spring and summer 2020 (see Fig. 8) varied more than those in 2021, with a lower diurnal cycle and generally stronger exponential decrease ($|\rho| \leq 0.4$ for $\Delta t \geq 4$ d vs. $\Delta t \geq 8$ d in spring, while $|\rho| \leq 0.4$ for $\Delta t \geq 4$ d vs. $\Delta t \geq 10$ d in summer, for 2020 and 2021, respectively).

Upon closer examination, coherence often dropped suddenly to low values during these periods (summer 2020). For example, when t_1 was set to 00:00 on and July 1 and 3, 2020, diurnal cycles were no longer observed after the end of the afternoon of July 2 and 5, respectively, [see Fig. 7(b)]. This large change was not due to electronic issues, agricultural activities, changes in vegetation cover or phenology, meteorological events, or irrigation events, the last of which were not detected in temporal signatures of coherence. The most likely origin may have been a large increase in soil roughness caused by animals, particularly wild boars, which farmers often observed. In contrast, no sudden drops were observed in 2021, when wild boars were hunted on the farm.

C. Baselines Corresponding to the Satellite Configuration

To analyze the potential of the Sentinel-1 configuration, coherence for baselines $\Delta t = t_2 - t_1 = 6$ d was estimated for the two Sentinel-1 acquisitions times over the study site (06:30 and 18:30) for the three two-month periods of 2021 (the more stable year). Median temporal signatures of $|\rho|$ were lower in the evening than in the morning, regardless of the period, due to higher W in the evening (see Fig. 9). In summer, which had the highest vegetation activity, coherence in the morning remained high ($|\rho| > 0.4$) for baselines $\Delta t \leq 8$ d and decreased to low and stable values ($|\rho| \approx 0.2$) for $\Delta t \geq 18$ d (see Fig. 9). A similar temporal signature was observed in the morning in spring and summer, with $|\rho|$ in spring of ca. 0.2 for $\Delta t \leq 18$ d (see Fig. 9). Similar behavior was observed during vegetation dormancy in autumn, whether in the morning or in the evening. This result is consistent with the previous observation that high nighttime

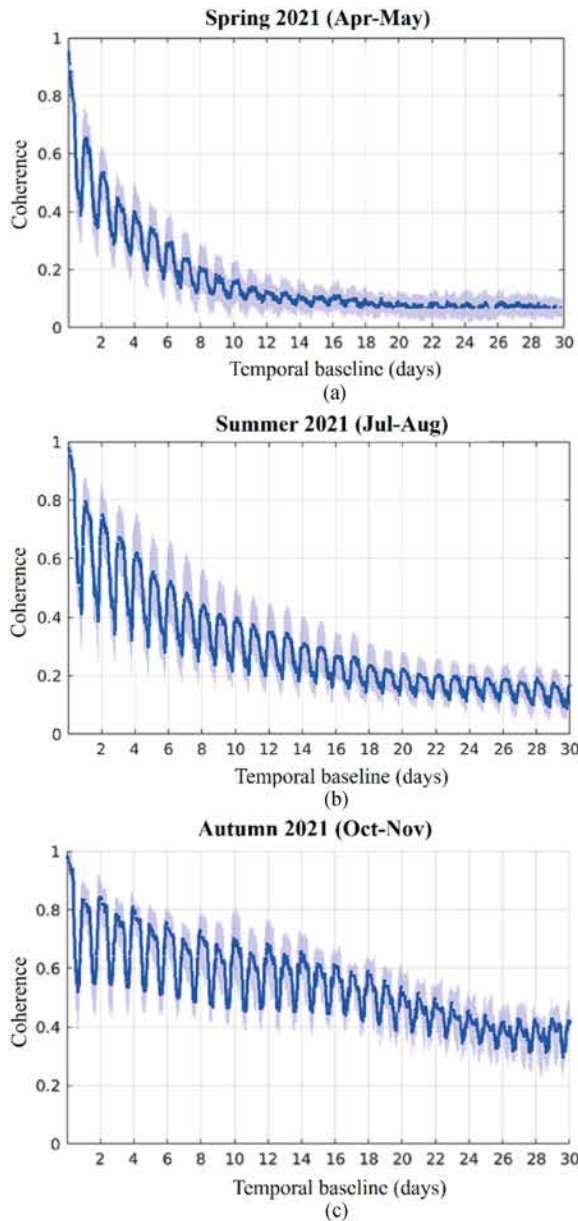


Fig. 6. Dynamics of the median coherence for increasing temporal baselines $\Delta t = t_2 - t_1$ of 0–30 d (with a time step of 15 min) for (a) April–May, (b) July–August and (c) October–November 2021. Variable t_1 was set to 00:00 on each day of the corresponding 2-month period. Light blue zones indicate 1 standard deviation.

plateau of $|\rho|$ were reached earlier in autumn due to a shorter period of wind each day (see Fig. 4).

To examine the influence of acquisition time, coherence was calculated for t_1 ranging from 00:00 to 23:45 with a time step of 15 min and temporal baselines of 1, 3, 6, 9, 12, and 18 d for the three two-month periods of 2021. The temporal signatures were generally the same as those observed previously, particularly for $\Delta t = 1$ d, including the multiple plateaus (at night for the entire period, and from 14:00–17:00 in the spring and summer); however, the mean of the median coherence and amplitude of the diurnal cycle decreased as the baseline increased [see Fig. 10].

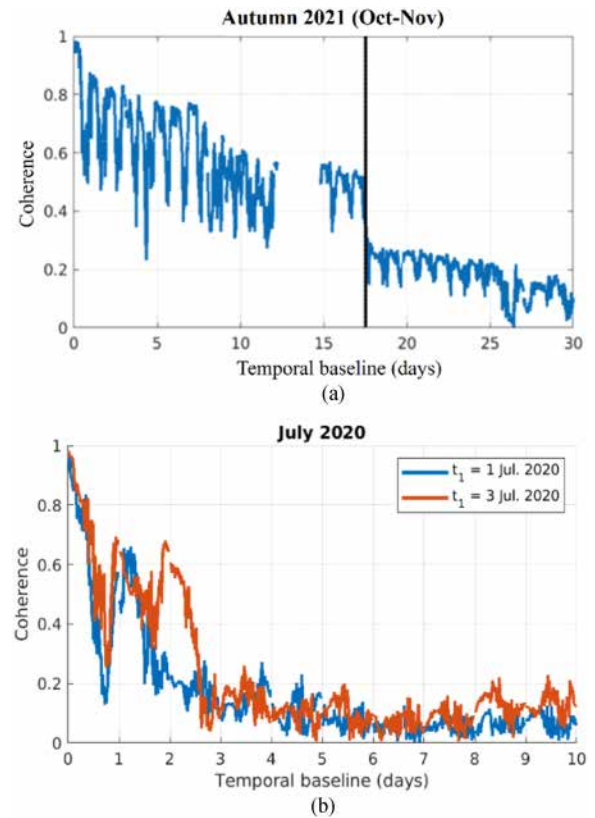


Fig. 7. Dynamics of coherence for increasing temporal baselines $\Delta t = t_2 - t_1$ of 0–30 d (with a time step of 15 min) for (a) $t_1 = 00:00$ on Oct. 25, 2021 (showing effects of the olive harvest (i.e., Nov. 11, dotted vertical line) for $t_2 = 17$ d) and (b) for $t_1 = 00:00$ on and Jul. 1 and 3, 2020 (showing a sudden drop at the end of and Jul. 2 and 5).

As before, coherence was lowest in spring, when vegetation was active, and highest in autumn, during dormancy. The diurnal signature remained strong in spring for $\Delta t = 6$ d (0.15–0.30), in summer for $\Delta t = 12$ d (0.20–0.35) and in autumn for $\Delta t \geq 18$ d (0.40–0.55), which indicates that the sentinel-1 configuration provides sufficiently sensitive estimates during the morning pass that could be related to the water status of vegetation. Indeed, when both Sentinel-1-A and -B satellites were operating, the temporal baseline $\Delta t = 6$ d provided coherence of 0.25–0.70, depending on the season.

These results naturally lead to compare the tower-based radar data to sentinel-1 data. Good date to date agreement was not expected since the two acquisition systems differed greatly in geometric configurations. For example, incidence angles of sentinel-1 orbits no. 52 and 118 were 35° and 45°, respectively, while those of the tower-based acquisitions were 40°–60°. Likewise, the azimuth look angle may also have influenced the comparison, since the tower-based radar line of sight was parallel to the rows of the olive orchard, but the sentinel-1 orbits ones were not.

We examined the time series of coherence with a 6-d temporal baseline estimated from both tower-based radar data and sentinel-1 data for orbits no. 52 and 118 (morning and evening

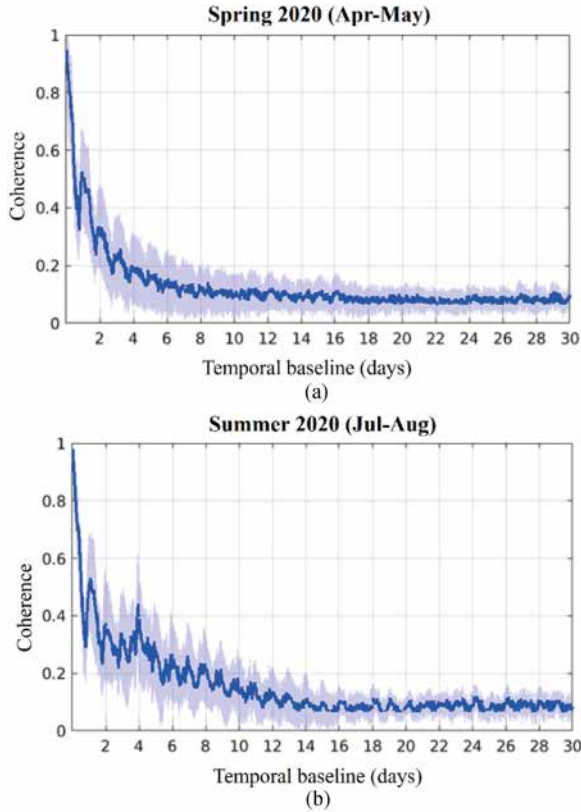


Fig. 8. Dynamics of the median coherence for increasing temporal baselines $\Delta t = t_2 - t_1$ of 0–30 d (with a time step of 15 min) for (a) April and May and (b) July and August 2020. Variable t_1 was set to 00:00 on each day of the corresponding two-month period. Light blue zones indicate 1 standard deviation. Data from October and November 2020 could not be used due to many power outages.

passes) from Mar. 2020 to Dec 2021. Overall, absolute and seasonal dynamics of tower-based radar data agreed well with Sentinel-1 data, with r^2 for VV and VH polarizations of 0.68 and 0.79, respectively, for orbit no. 52 and 0.74 and 0.83, respectively, for orbit no. 118 (see Fig. 11). When VV and VH polarizations of Sentinel-1 data were merged, r^2 was 0.79 and 0.83 for orbits no. 52 and 118, respectively. Coherence decreased in spring and summer, when vegetation was growing, and increased in autumn and winter, when vegetation was dormant and W was lower; the lowest coherence was observed in spring for VH polarizations. Minimum values of coherence were lower for tower-based acquisitions (≈ 0.1) than for sentinel-1 data (≈ 0.2), 0.2 having already been observed as a minimum for sentinel-1 data over temperate forest [20]. Sentinel-1 coherence varied greatly in autumn and winter 2020, but unfortunately, tower-based sensors were not operating at that time. Absolute values of coherence for sentinel-1 data did not differ significantly between morning and evening passes, or between VV and VH polarizations (for the latter, r^2 was 0.74 and 0.86 for orbits no. 52 and 118, respectively), except in spring and summer 2021. Nevertheless, VH showed lower values than VV ($\rho_{VH} \leq 0.6$ and $\rho_{VV} \leq 0.8$, and an overall average over the whole study period equal to 0.33 and 0.45, respectively). Finally, it can be noted that

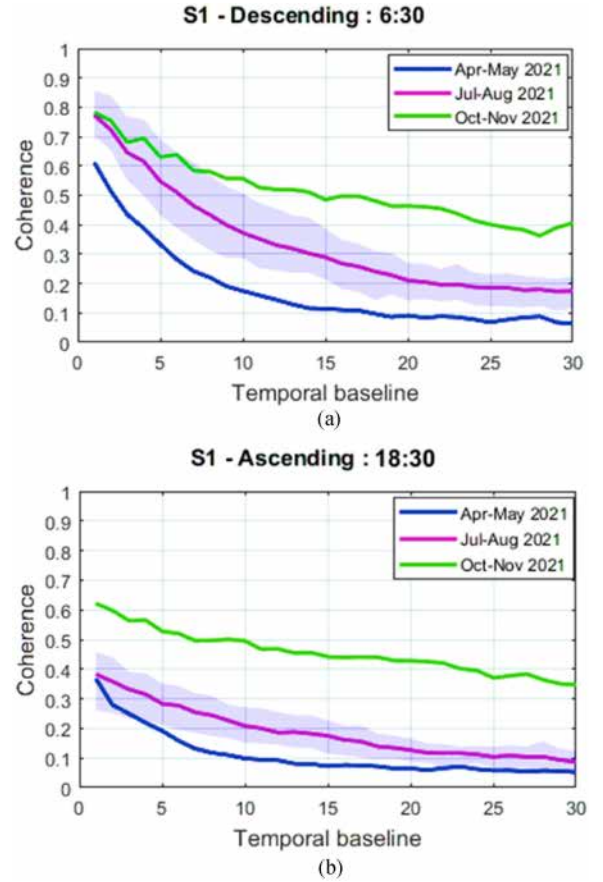


Fig. 9. Dynamics of median coherence for increasing baselines $\Delta t = t_2 - t_1$ from 1–30 d (with a time step of 1 d) for three two-month periods (a) at 06:30 and (b) 18:30. Light blue zones indicate 1 standard deviation.

coherence of both systems had similar seasonal dynamics, while that of sentinel-1 data had lower annual amplitudes

IV. DISCUSSION

This article demonstrates high sensitivity of coherence to W and the physiological functioning of crop trees, which was highlighted for the first time using measurements from the monitoring of plant physiology (i.e., sapflow and trunk circumference). Several results support the potential sensitivity of $|\rho|$ to the physiology and structure of vegetation; for example, a large drop in coherence coincided with the olive harvest, and the morning coherence drop coincided with the onset of diurnal cycles of sapflow and ETR. In addition, correlations between $|\rho|$ and ETR, sapflow or the daily residual variation in tree circumference were strong when W was low, which can be attributed to the sensitivity of $|\rho|$ to the water content of vegetation, even though these parameters are indirectly related to it. Nevertheless, this hypothesis remains difficult to support, since these three physiological parameters did not directly measure the water content of vegetation. However, this hypothesis is the most probable given the sensitivity of microwaves to the dielectric constant of plant matter, as highlighted by many studies [10], [11], [13], [38]. Previous studies using tower-based acquisitions installed

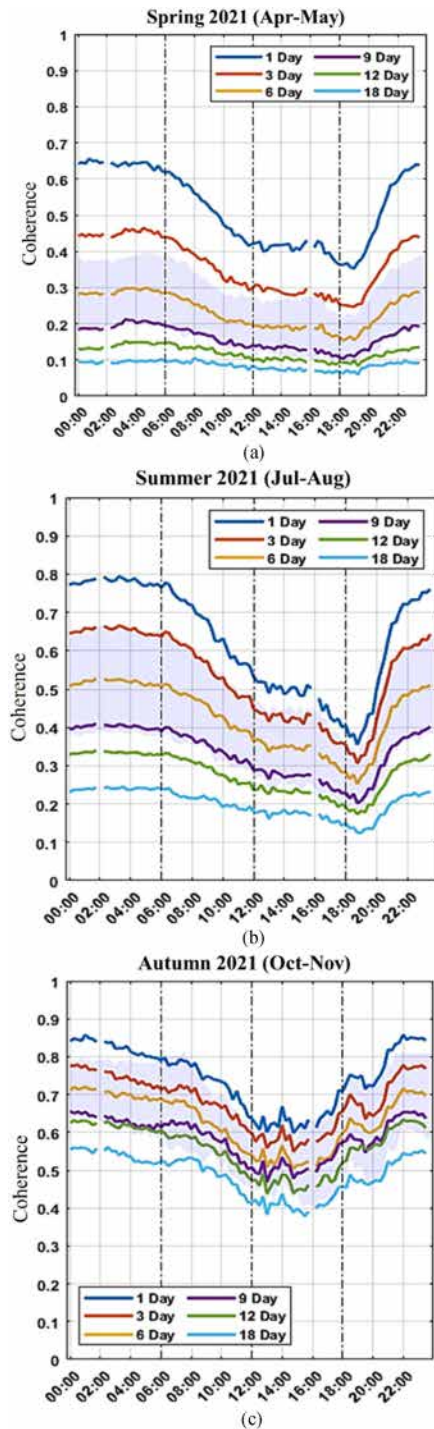


Fig. 10. Diurnal cycle of the median coherence estimated for baselines $\Delta t = 1, 3, 6, 9, 12$ and 18 d for (a) April and May, (b) July and August (c) October and November 2021. Light blue zones indicate 1 standard deviation for $\Delta t = 6$ d.

over BF [19] or TFs [17], [18], [19], [20] hypothesized this sensitivity to vegetation physiology. However, the diurnal cycles of coherence of the olive orchard differed from those of BF and TF. First, the morning coherence drop was smoother than that of TF, most likely due to lower ETR: the evaporative demand (ET₀), calculated using the FAO Penman–Monteith equation [39], was

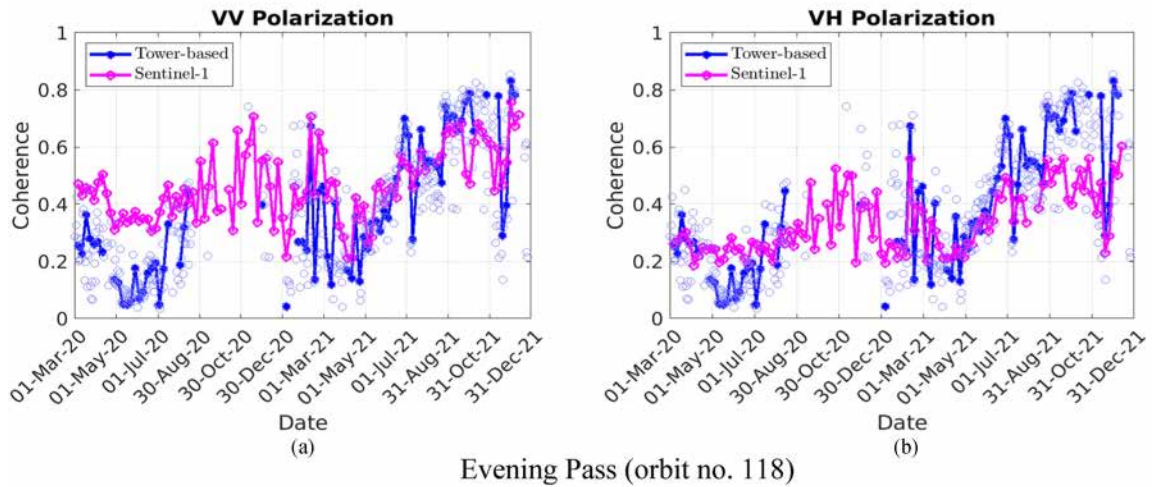
0.4–0.6 mm/h in the present study versus 1.25 mm/h for TF. In addition, the olive orchard had a minimum coherence (≈ 0.4) higher than those of TF and BF (≈ 0.2), which could indicate that it (having relatively sparse vegetation) had more ground contribution than did TF, which had a cover fraction close to 1. The strong decrease in coherence in spring and summer 2020, likely related to an increase in soil roughness, could support the hypothesis of more ground contribution. Surprisingly, coherence was not sensitive to irrigation events, likely because the drip irrigation system installed on the study field irrigated a small fraction of the soil along the row at the base of the trunks, while the rest of it remained dry.

When the temporal baseline increased, relatively high coherence was still observed after several days. In 2021, which did not experience the disturbances observed in 2020, coherence was high after 12 d in summer and 6 d in spring. In spring, when tree growth was strong, the decrease in coherence as with Δt increased was higher, but the diurnal cycle was still discernable, although the amplitude was lower than that in summer. The diurnal cycle, still observed for multi-day baselines, explains the seasonal variations of sentinel-1 coherence. There is little difference between sentinel-1 coherence derived from measurements acquired during morning and evening passes, with the exception of summer 2021, when the former are higher. It is in fact during the summer that the diurnal cycle is most pronounced. Similarly, sentinel-1 coherence in VV and VH polarizations, show overall similar behaviors with strong observed correlations. But observed small differences are difficult to interpret: lower VH coherence values and different behavior during spring and summer 2021, as tower-based acquisitions do not show any significant differences. This point is currently under discussion and will be subject of future work. These results show that coherence may be useful for monitoring vegetation using configurations such as those of the sentinel-1 missions (especially when both satellites are operating, which provides a revisit time of 6 d). They are also of interest for future spaceborne missions, such as the geostationary HydroTerra mission [40], which will acquire radar data with temporal baselines of several minutes.

V. SUMMARY AND CONCLUSION

The main objective of this article was to assess factors that influenced the diurnal cycle of the temporal coherence in an irrigated olive orchard. To this end, this article investigated the behavior of $|\rho|$ estimated from C-band radar data over an olive orchard in a semiarid Mediterranean environment. The data were recorded quasi-continuously by a tower-based radar system with a time step of 15 min from March 2020 to December 2021. Temporal dynamics of coherence were analyzed using baselines of 0–30 d (with a time step of 15 min) for three two-month periods that corresponded to different phenological stages. Coherence dropped suddenly during the olive harvest, as well as regularly in spring and summer 2020, most likely due to large changes in soil roughness, which illustrate the sensitivity of coherence to vegetation and the ground for such sparse tree cover. The present article confirms previous observations of TF and BF in summer

Morning Pass (orbit no. 52)



Evening Pass (orbit no. 118)

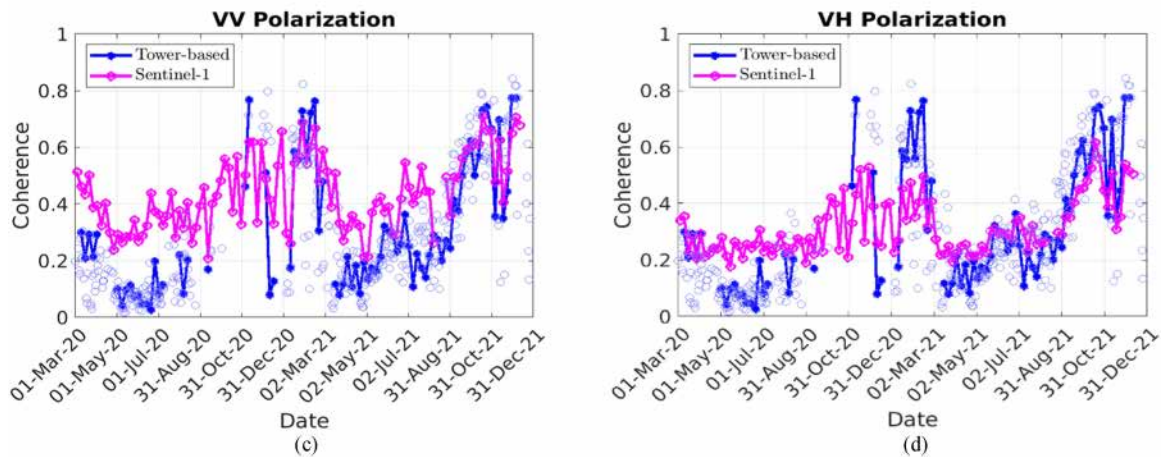


Fig. 11. Coherence (with $\Delta t = 6$ d) estimated from tower-based radar data (TR) or sentinel-1 data for (top) morning ($\theta = 35^\circ$) and (bottom) evening ($\theta = 45^\circ$) passes, for (left) VV and (right) VH polarizations. Blue empty circles correspond to all TR acquired at the same time of day (top: 06:30, bottom: 18:30), while full blue stars correspond to TR acquired on the same days as sentinel-1 data.

(i.e., the sensitivity of $|\rho|$ to scatterer movement due to the wind, as well as to the activity of vegetation, which has a large diurnal cycle when 15-min baselines are considered, especially in spring and summer). This article goes beyond pioneering studies by providing quantitative data that support the relation between the morning coherence drop and the water status of plants, using measurements directly related to plant physiology and water status. The temporal drop rate of coherence was significantly related to the daily residual variation in trunk circumference.

For long temporal baselines, the diurnal cycle remained significant up to 6, 12, and more than 18 d in spring, summer and winter, respectively. Overall, temporal profiles estimated by tower-based versus sentinel-1 data from March 2020 to December 2021 agreed well at the seasonal scale, regardless of the acquisition time (morning or evening). However, they sometimes differed greatly, especially in summer 2020 and summer-autumn 2021, which were difficult to analyze due to large differences in their incidence angles (and possibly azimuth

angles), as well as in polarization, which could not be unmixed for tower-based measurements.

These results open perspectives for monitoring the water status of tree crops using C-band satellite radar data. In particular, early morning acquisitions are sensitive to the onset of water activity of the vegetation, especially during seasons with phenological stages that are crucial for olive production (i.e., spring and summer). They show that the acquisition times and temporal baseline of the sentinel-1 mission are appropriate, although a temporal baseline of 6 d is the maximum that can capture the diurnal cycle of vegetation in summer. The ability to obtain additional measurements from other spaceborne sensors in the early morning would allow for deeper analysis of using the slope of the morning coherence as a proxy for estimating the water status of vegetation. These results may also be useful for future geostationary spaceborne missions such as HydroTerra, which will provide baselines of several minutes. In the longer term, we would like to assess the ability to use coherence for

early detection of water stress in order to improve irrigation scheduling and rationalize the use of agricultural water in these water-scarce regions

ACKNOWLEDGMENT

The authors gratefully acknowledge these institutions for their generous financial assistance and support. The authors also thank Dr. O. Rafi, the owner of the private farm where the study site was located.

REFERENCES

- [1] M. Hoerling, J. Eischeid, J. Perlwitz, X. Quan, T. Zhang, and P. Pegion, "On the increased frequency of Mediterranean drought," *J. Climate*, vol. 25, no. 6, pp. 2146–2161, Mar. 2012.
- [2] Y. Trambly et al., "Challenges for drought assessment in the Mediterranean region under future climate scenarios," *Earth Sci. Rev.*, vol. 210, Nov. 2020, Art. no. 103348.
- [3] M. Fader, S. Shi, W. Von Bloh, A. Bondeau, and W. Cramer, "Mediterranean irrigation under climate change: More efficient irrigation needed to compensate for increases in irrigation water requirements," *Hydrol. Earth System Sci.*, vol. 20, no. 2, pp. 953–973, Mar. 2016.
- [4] Y. Ouassanouan et al., "Multi-decadal analysis of water resources and agricultural change in a Mediterranean semiarid irrigated piedmont under water scarcity and human interaction," *Sci. Total Environ.*, vol. 834, Aug. 2022, Art. no. 155328.
- [5] L. S. Pereira, "Challenges on water resources management when searching for sustainable adaptation to climate change focusing agriculture," *Eur. Water*, vol. 34, pp. 113–124, 2011.
- [6] L. S. Pereira, T. Oweis, and A. Zairi, "Irrigation management under water scarcity," *Agricultural Water Manage.*, vol. 57, no. 3, pp. 175–206, Dec. 2002.
- [7] G. Boulet, A. Chehbouni, P. Gentile, B. Duchemin, J. Ezzahar, and R. Hadria, "Monitoring water stress using time series of observed to unstressed surface temperature difference," *Agricultural Forest Meteorol.*, vol. 146, no. 3–4, pp. 159–172, Oct. 2007.
- [8] N. Ouadi et al., "Monitoring of wheat crops using the backscattering coefficient and the interferometric coherence derived from sentinel-1 in semi-arid areas," *Remote Sens. Environ.*, vol. 251, Dec. 2020, Art. no. 112050.
- [9] J. D. Kalma, T. R. McVicar, and M. F. McCabe, "Estimating land surface evaporation: A review of methods using remotely sensed surface temperature data," *Surv. Geophys.*, vol. 29, no. 4, pp. 421–469, Aug. 2008.
- [10] F. T. Ulaby, "Radar response to vegetation," *IEEE Trans. Antennas Propag.*, vol. 23, no. 1, pp. 36–45, Jan. 1975, doi: 10.1109/TAP.1975.1140999.
- [11] F. T. Ulaby, T. F. Bush, and P. P. Batlivala, "Radar response to vegetation II: 8–18 GHz band," *IEEE Trans. Antennas Propag.*, vol. 23, no. 5, pp. 608–618, Sep. 1975, doi: 10.1109/TAP.1975.1141133.
- [12] J. Sweet and G. Berthold, " σ^0 signature of the amazon rain forest obtained from the seasat scatterometer," *IEEE Trans. Geosci. Remote Sens.*, vol. 20, no. 1, pp. 11–17, Jan. 1982, doi: 10.1109/TGRS.1982.4307513.
- [13] S. C. Steele-Dunne, J. Friesen, and N. Van De Giesen, "Using diurnal variation in backscatter to detect vegetation water stress," *IEEE Trans. Geosci. Remote Sens.*, vol. 50, no. 7, pp. 2618–2629, Jul. 2012, doi: 10.1109/TGRS.2012.2194156.
- [14] P. L. Frison et al., "Potential of sentinel-1 data for monitoring temperate mixed forest phenology," *Remote Sens.*, vol. 10, no. 12, 2018, Art. no. 2049.
- [15] A. Veloso et al., "Understanding the temporal behavior of crops using sentinel-1 and sentinel-2-like data for agricultural applications," *Remote Sens. Environ.*, vol. 199, 2017, Art. no. 25021.
- [16] P. L. Frison et al., "C band radar crops monitoring at high temporal frequency: First results of the MOCTAR campaign," in *Proc. Mediterranean Middle-East Geosci. Remote Sens. Symp.*, 2020, pp. 310–313.
- [17] A. Hamadi, L. Villard, P. Borderies, C. Albinet, T. Koleck, and T. Le Toan, "Comparative analysis of temporal decorrelation at P-band and low L-band frequencies using a tower-based scatterometer over a tropical forest," *IEEE Geosci. Remote Sens. Lett.*, vol. 14, no. 11, pp. 1918–1922, Nov. 2017, doi: 10.1109/LGRS.2017.2731658.
- [18] L. Villard, T. Le Toan, D. H. Tang Minh, S. Mermoz, and A. Bouvet, "Forest biomass from radar remote sensing," *Land Surf. Remote Sens. Agriculture Forest*, vol. 3, pp. 363–425, 2016.
- [19] S. El Idrissi Essebtey et al., "Temporal decorrelation of tropical dense forest at C-band: First insights from the TropiScat-2 experiment," *IEEE Geosci. Remote Sens. Lett.*, vol. 17, no. 6, pp. 928–932, Jun. 2020, doi: 10.1109/LGRS.2019.2937382.
- [20] S. E. I. Essebtey, L. Villard, P. Borderies, T. Koleck, B. Burban, and T. Le Toan, "Comparative study of temporal decorrelation at P, L and C-bands: First insights from the tropiscat-2 experiment," in *Proc. Mediterranean Middle-East Geosci. Remote Sens. Symp.*, 2020, pp. 1–6.
- [21] A. R. Monteith and L. M. H. Ulander, "A tower-based radar study of temporal coherence of a boreal forest at P-, L-, and C-bands and linear cross polarization," *IEEE Trans. Geosci. Remote Sens.*, vol. 60, May 2022, Art. no. 4402315, doi: 10.1109/TGRS.2021.3074098.
- [22] L. Jarlan et al., "Remote sensing of water resources in semi-arid mediterranean areas: The joint international laboratory TREMA," *Int. J. Remote Sens.*, vol. 36, no. pp. 19–20, 2015.
- [23] A. Abourida, V. Simonneaux, E. Sadik, B. Brahim, and S. Fathallah, "Estimation des volumes d'eau pompés dans la nappe pour l'irrigation (plaine du Haouz, Marrakech, Maroc). Comparaison d'une méthode statistique et d'une méthode basée sur l'utilisation de la télédétection," *Revue des Sci. de l'Eau / J. Water Sci.*, vol. 22, no. 1, 2009, Art. no. 2363.
- [24] F. Eder, F. De Roo, E. Rotenberg, D. Yakir, H. P. Schmid, and M. Mauder, "Secondary circulations at a solitary forest surrounded by semi-arid shrubland and their impact on eddy-covariance measurements," *Agricultural Forest Meteorol.*, vol. 31, vol. pp. 211–212, 2015.
- [25] A. Granier, "Une nouvelle méthode pour la mesure du flux de sève brute dans le tronc des arbres," *Ann. Forest Sci.*, vol. 42, no. 2, pp. 193–200, 1985.
- [26] C. Charfi Masmoudi, M. Masmoudi, J. Abid-Karray, and N. Ben Mechlia, "Sap flow measurements in young olive trees (olea Europaea L.) cv. Chétoui under tunisian conditions," *Scientia Horticulturae*, vol. 129, no. 4, pp. 235–256, 2011.
- [27] F. Do and A. Rocheteau, "Influence of natural temperature gradients on measurements of xylem sap flow with thermal dissipation probes. 2. Advantages and calibration of a noncontinuous heating system," *Tree Physiol.*, vol. 22, no. 9, pp. 649–654, Jun. 2002.
- [28] R. Core Team, "R: A language and environment for statistical computing," 2022. [Online]. Available: <https://www.R-project.org/>
- [29] S. Aryal, M. Häusser, J. Grießinger, Z. Fan, and A. Bräuning, "'dendRoAnalyst': A tool for processing and analysing dendrometer data," *Dendrochronologia*, vol. 64, Dec. 2020, Art. no. 125772.
- [30] "S5065 2-Port 6.5 GHz analyzer - Copper mountain technologies," Accessed on: Mar. 30>, 2023. [Online]. Available: <https://coppermountaintech.com/vna/s5065-2-port-6-5-ghz-analyzer/>
- [31] J. - S. Lee and E. Pottier, *Polarimetric Radar Imaging: From Basics to Applications*. Boca Raton, FL, USA: CRC Press, 2009.
- [32] S. El Idrissi Essebtey, L. Villard, P. Borderies, T. Koleck, B. Burban, and T. Le Toan, "Long-term trends of P-band temporal decorrelation over a tropical dense forest-experimental results for the BIOMASS mission," *IEEE Trans. Geosci. Remote Sens.*, vol. 60, Jun. 2022, Art. no. 5102415, doi: 10.1109/TGRS.2021.3082395.
- [33] D. Massonnet and J. C. Souyris, *Imaging With Synthetic Aperture Radar*. Boca Raton, FL, USA: CRC Press, 2008.
- [34] R. Touzi, A. Lopes, J. Bruniquel, and P. W. Vachon, "Coherence estimation for SAR imagery," *IEEE Trans. Geosci. Remote Sens.*, vol. 37, no. 1, pp. 135–149, Jan. 1999, doi: 10.1109/36.739146.
- [35] "SNAP : Sentinel applications platform. Available online : (accessed on 10th Oct. 2022)," 2022, Accessed on: Oct. 17, 2022. [Online]. Available: <https://step.esa.int/main/toolboxes/snap>
- [36] K. M. Herzog, R. Häslér, and R. Thum, "Diurnal changes in the radius of a subalpine Norway spruce stem: Their relation to the sap flow and their use to estimate transpiration," *Trees: Struct. Function*, vol. 10, no. 2, pp. 94–101, Dec. 1995.
- [37] J. E. Fernández and M. V. Cuevas, "Irrigation scheduling from stem diameter variations: A review," *Agricultural Forest Meteorol.*, vol. 150, no. 2, pp. 135–151, 2010.
- [38] T. Van Emmerik, S. C. Steele-Dunne, J. Judge, and N. Van De Giesen, "Impact of diurnal variation in vegetation water content on radar backscatter from maize during water stress," *IEEE Trans. Geosci. Remote Sens.*, vol. 53, no. 7, pp. 3855–3869, Jul. 2015, doi: 10.1109/TGRS.2014.2386142.
- [39] R. G. Allen, L. S. Pereira, D. Raes, and M. Smith, *Crop Evapotranspiration - Guidelines for Computing Crop Water Requirements - FAO Irrigation and Drainage Paper 56*. Dehradun, Uttarakhand: Irrigation Drainage, 1998.
- [40] S. E. Hobbs et al., "G-CLASS: Geosynchronous radar for water cycle science – Orbit selection and system design," *J. Eng.*, vol. 2019, no. 21, pp. 7534–7537, Nov. 2019.



Adnane Chakir received the master's degree in engineering of solar thermal systems in 2019 from Cadi Ayyad University, Marrakesh, Morocco, where he is currently working toward the Ph.D. degree in the use of radar for detecting water stress over olive and wheat canopies in Morocco.

He works on the use of radar for detecting water stress over olive and wheat canopies in Morocco.



Pascal Fanise received the M.Sc. degree in electronic engineering from the University of Paris XII, Créteil, France, in 2003.

Since 2010, he has been with the Centre D'études Spatiales de la Biosphère, Toulouse, France, where he is currently an Instrumentation Engineer and a Technical Manager for several ground-based and airborne instruments. He is currently responsible for the design of the hardware architecture and experiment for the GLORI reflectometer. His research focuses on microwave radiometer systems.



Pierre-Louis Frison received the M.S. degree in astrophysics, geophysics, and spatial techniques and the Ph.D. degree in remote sensing from University Paul Sabatier, Toulouse, France, in 1993 and 1997, respectively.

He is currently Assistant Professor with University Gustave Eiffel, Marne la Vallée, France. He carries out his research work at LaSTIG on the monitoring of land surfaces by remote sensing, and more specifically on the monitoring of vegetation by radar sensors. Since October 2022, as part of his delegation

to the IRD at CESBIO, he is assigned to the TREMA laboratory at Cadi Ayyad University, Marrakech, Morocco, until September 2024.



Khabba Saïd received the Ph.D. degree in water sciences from Cadi Ayyad University, Marrakech, Morocco, in 2000.

He has been a Senior Lecturer with the Faculty of Sciences Semlalia, Cadi Ayyad University, since 1996. He is an Eco-Physiologist and has a background in agro-climatology and modeling. He has key expertise in micrometeorology and crops water requirement. The approach used is based on the synergy between field measurements, simple and complex modeling, and satellite observations (multisensor and multiresolution). He has authored and coauthored more than 100 papers in international peer-reviewed journals and has supervised 11 Ph.D. students. His research interest includes modeling crop growth, development, and yield in semiarid areas.



Ludovic Villard received the engineering degree from ENAC (National School of Civil Aviation), Toulouse, France, in 2005, the research master degree in microwave and telecommunications from the Paul Sabatier University, Toulouse, France, in 2005, and the Ph.D. degree, with thesis in on forward and inverse modeling of bistatic SAR observables with applications on forest remote sensing, from the National School of Aeronautics and Space (ISAE-Supaero), Toulouse, in 2009.

During the Ph.D. thesis, he was with ONERA (the French Aerospace Lab, Toulouse) and for about one year with DLR (German Aerospace Center, Oberpfaffenhofen). His research focuses on the development of forest biomass retrieval algorithms from SAR data.

Dr. Villard was the recipient of Postdoctoral Grant from the Centre National d'Etudes Spatiales in 2010. He currently conducts research works at the Centre d'Etudes Spatiales de la Biosphère in the frame of the BIOMASSmission supporting activities.



Valérie Le Dantec received the M.S. degree in biology and ecophysiology and the Ph.D. degree in ecophysiology from the University Paris XI (Paris-Saclay), Orsay, France, in 1995 and 2000, respectively.

Since 2001, she has been an Associated Professor with the University Toulouse 3—Paul Sabatier, Toulouse, France. She works on the potentialities of remote sensing to detect water stress in agrosystems.



Nadia Ouaadi received the B.S. degree in mathematics, computer science, and physics from the Faculty of Sciences and Techniques, Sultan Moulay Slimane University, Beni Mellal, Morocco, in 2015, the M.S. degree in mechanics of fluids and energetics from the Faculty of Sciences Semlalia, Cadi Ayyad University, Marrakesh, Morocco, in 2017, and the Ph.D. degree in remote sensing and water resources management jointly from Paul Sabatier University, Toulouse, France, and Cadi Ayyad University, Marrakech, Morocco, in 2021.

She is currently a Postdoctoral Researcher with the French National Center for Scientific Research and has been with the Center for the Study of the Biosphere from Space since 2021. She is working on the processing and exploitation of SAR polarimetry and interferometry data for monitoring the hydric conditions of annual crops.



Rafi Zoubair received the licence of fundamental studies in physical sciences, energy pathway from the Faculty of Sciences Semlalia of the University of Cadi Ayyad in Marrakech, Morocco, in 2013, the master's degree in water sciences from the Faculty of Sciences Semlalia, Cadi Ayyad University, Marrakesh, Morocco, in 2016 and the Ph.D. degree in remote sensing and water resources management from the Université Paul Sabatier in Toulouse, France, and Cadi Ayyad University.

Since 2022, he has been a Postdoctoral Researcher with the Institute for Research and Development, Marrakesh, Morocco. He is working on the research and development of real-time satellite tools for irrigation monitoring and scheduling in Morocco



Jamal Ezzahar received the Ph.D. degree in physics from the Faculty of Sciences Semlalia, Cadi Ayyad University, Marrakesh, Morocco, in 2007.

He is currently a Permanent Professor with the Department of Computer Science, Networks and Telecommunications, National School of Applied Sciences Safi, Safi, Morocco. His research interests include soil moisture, turbulent fluxes, machine learning, multisource remote sensing imagery, and coupled land-atmosphere systems modeling for land applications in semiarid regions.



Bénédictte Fruneau received the B.S. degree in electrical engineering and the M.Sc. degree in image and signal processing from the Grenoble Institute of Technology, Grenoble, France, in 1991, and the Ph.D. degree in geophysics from the University of Paris 7, Paris, France, in 1995.

Since 1996, she has been with the University Paris-Est Marne-la-Vallée, Marne-la-Vallée, France, where she is currently an Associate Professor. Her research activities are principally dedicated to the measurement and the analysis of surface deformation

associated with natural or anthropogenic phenomena in various contexts using SAR differential interferometry and persistent scatterers interferometry.



Jean-Paul Rudant received the Aggregation in physics from the Ministère de l'Éducation Nationale, Paris, France, in 1969 and the Ph.D. degree in geophysics from the Pierre et Marie Curie University, Paris, France, in 1974.

He was a Professor with the University Paris-Est Marne la Vallée, Marne la Vallée, France. His experience covers geophysics and remote sensing. He supervised the Geographical Information Master co-empowered with the École Nationale des Sciences Géographiques until 2015. He has invested in numerous

programs with space agencies, such as Centre National d'Études Spatiales, European Space Agency, and the National Space Development Agency of Japan, involving radar images. More recently, he has invested in the dissemination of educational university resources on radar imagery, free of access to remote sensing within ENSG, European Space Agency, Copernicus Research and EOCollege of Jena-University.



Jarlan Lionel received the Ph.D. degree in remote sensing and the “habilitation” from Paul Sabatier University, Toulouse, France, in 2001 and 2016, respectively.

Since 2006, he has been a Research Scientist with the French Research Institute for Sustainable Development, Center for Spatial Studies of the Biosphere, Toulouse, France. His work is focused on the monitoring of water resources, of the agricultural water uses, and their evolution under the influence of global changes by combining spatial observation data with

ecohydrological modeling. He is currently working on new methods based on multi-spectral remote sensing for the early detection of water stress in agricultural crops to improve irrigation management. He co-authored about 100 papers in peer-reviewed journal.